
Proceedings Paper:
Priest, J., Ghadbeigi, H., Ayvar-Soberanis, S. orcid.org/0000-0002-1899-9743 et al. (2 more authors) (2022) A modified Johnson-Cook constitutive model for improved thermal softening prediction of machining simulations in C45 steel. In: Rech, J. and Outeiro, J., (eds.) Procedia CIRP. 6th CIRP Conference on Surface Integrity, 08-10 Jun 2022, Lyon, France. Elsevier BV , pp. 106-111.

https://doi.org/10.1016/j.procir.2022.03.022

Available online at www.sciencedirect.com

ScienceDirect

Procedia CIRP 108 (2022) 106–111

www.elsevier.com/locate/procedia

6th CIRP Conference on Surface Integrity

A modified Johnson-Cook constitutive model for improved thermal softening prediction of machining simulations in C45 steel

Joshua Priest[a,b]*, Hassan Ghadbeigi[b], Sabino Ayvar-Soberanis[c], Anders Liljerehn[d], Matthew Way[e]

[a] *Industrial Doctoral Centre in Machining Science, Advanced Manufacturing Research Centre with Boeing, University of Sheffield, Rotherham, S60 5TZ, UK*
[b] *The University of Sheffield, Department of Mechanical Engineering, Sir Fredrick Mappin Building, Mappin Street, S1 3JD, Sheffield, UK*
[c] *Advanced Manufacturing Research Centre with Boeing, Advanced Manufacturing Park, Catcliffe, Rotherham, S60 5TZ, UK*
[d] *Sandvik Coromant AB, Mossvägen 10, Sandviken, Sweden*
[e] *Sandvik Coromant AB , Unit 8, Morse Way, Waverley, Rotherham, S60 5BJ, UK*

* Corresponding author. Tel.: N/A ; fax: N/A. *E-mail address:* j.priest@amrc.co.uk

Abstract

A new modified Johnson-Cook model is developed to capture the non-linear thermal softening behaviour below the austenite transformation temperature (723°C) in C45 ferritic-pearlitic steel, which is not captured by the original Johnson-Cook (JC) model. The physical mechanisms responsible for this behaviour are also studied. The model is developed by experimental quasi-static and high strain rate axisymmetric compression testing from 20°C to 720°C and implemented into 3D finite element drilling simulations. The improvement over the original JC model is demonstrated by comparison to experimentally measured torque and thrust force.

Keywords: C45; machining; Johnson-Cook

1. Introduction

In metal cutting simulations, it is critical that an accurate model of the material constitutive response is used to capture the plastic deformation of the workpiece. There are two categories of material constitutive plasticity models that are implemented into finite element (FE) machining simulations, phenomenological and physics-based models. Phenomenological models are formulated through empirically fitted equations with respect to variables such as the strain, strain rate, and temperature; whereas physical models are based on the physical mechanisms responsible for strengthening and softening [1]. The primary hardening mechanism in ferritic-pearlitic steels is dislocation-obstacle interaction, while softening is driven by dynamic recovery and dynamic recrystallisation.

The most popular phenomenological model used for metal cutting simulations in C45 is the Johnson-Cook (JC) strain, strain-rate, and temperature-dependent constitutive model [2]. This model has been shown to fit very well with experimental stress-strain data within the same ranges of strain, strain rate, and temperature as the data used to tune the model parameters [3].

Jaspers and Dautzenberg [4] demonstrated that the physically based Zerilli-Armstrong model predicted the flow stress of C45 much better than the JC model at strain rates up to 7500 s^{-1} and temperatures up to 700°C. However, the errors in both models compared to the experimental flow stress were not significant. In contrast, another study demonstrated that the JC model was superior to the physically-based Zerilli-Armstrong and Mechanical Threshold Stress models when compared with experimental flow stress data at temperatures up to 1000°C at a strain-rate of 5000 s^{-1} [3].

10.1016/j.procir.2022.03.022

However, the limitations of the JC model have been highlighted by many researchers, these are primarily the inability to predict some of the physical hardening phenomena such as dynamic strain ageing (DSA) [5] and softening phenomena such as dynamic re-crystallisation (DRX) [6] which occurs in C45 steel in the high-temperature deformation regimes. DSA increases the resistance to dislocation movement caused by the mobility of solute atoms that diffuse to dislocation sites above certain temperatures, resulting in increased strength [7].

Courbon et al. [6] demonstrated the formation of DRX in the secondary shear zone during high-speed orthogonal cutting and developed a material model to account for this. This used the Voce model [8] to predict the work hardening and dynamic recovery, with a term to reduce the flow stress in the DRX regime. This was then implemented into orthogonal cutting simulations, although the predicted cutting forces and chip thicknesses were similar to those predicted using the JC model.

Bleicher et al. [9] developed a physically based material model for AISI 1045 (C45E equivalent) that uses the Voce hardening model to capture the temperature and strain-rate effects of hardening, and a gaussian function to capture the DSA effects. The cutting force and chip morphology were better predicted in orthogonal cutting at higher cutting speeds, although, this was not a significant improvement over the JC model. Devotta et al. [5] modified the JC model strain hardening term to capture this DSA effect at strain rates up to 60 s^{-1}, which showed a significant improvement over the JC model in the DSA regime between 200 - 400°C at the expense of adding an additional 10 empirical parameters to be tuned. A similarly modified JC model was implemented into orthogonal cutting simulations with a modified damage model, which was shown to improve the cutting force prediction compared with the original JC model [10].

This study aims to characterise the C45 non-linear thermal softening effects in the 200 - 400°C temperature regime in more depth. This is achieved through high-temperature isothermal compression testing and metallographic analysis of the material after deformation which has not been discussed in the previous literature. This behaviour is then captured by developing a novel modified JC model with a reduced number of empirical parameters compared to the models in the literature. This model is then implemented into 3D FE drilling simulations to determine the efficacy compared with the original JC model.

2. Experimental Methodology

The material used in this study is an annealed C45U steel with the chemical composition shown in Table 1. The as-received material consisted of uniform ferritic-pearlitic microstructure with coarse perlite grains due to the annealing process as demonstrated by scanning electron (SEM) micrographs in Fig. 1a and Fig. 1b.

Table 1. Chemical composition of C45U annealed material used in this study.

C	Si	Mn	P	S
0.48	0.280	0.740	0.01	0.03

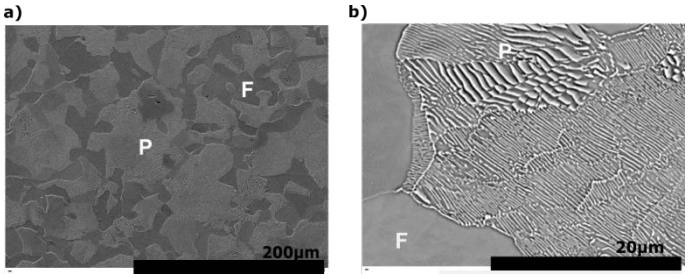

Fig. 1. SEM micrographs of the base annealed C45U material. F and P demonstrate a ferrite and pearlite grain, respectively.

2.1. High-temperature compression testing

Isothermal high-temperature axis-symmetric compression testing was carried out using cylindrical samples with a 10 mm diameter and 15 mm length. A 1.1 mm Type N thermocouple was inserted into the centre of the sample, through the drilled hole, to ensure the required testing temperature is reached and recorded during deformation.

Strain rates of 0.1 s^{-1} (quasi-static condition) and 10 s^{-1} were used at temperatures from 20 to 720ºC to determine the effect of temperature on the flow stress of the material. Fl

Each test condition was repeated 3 times. The samples are heated up to the testing temperature at a rate of 10 °C/s and then held at the testing temperature for 120 seconds to allow the temperature to stabilise. After this soak time the compression test was performed, followed by quenching of the sample to room temperature a rate of 100 °C/s with a water mist spray.

The applied total strain was varied depending on the testing temperature to achieve uniform plastic deformation and prevent the failure of the sample due to fracture. Table 2 shows the applied engineering strains at different testing conditions.

Table 2. Test matrix for the high-temperature compression testing, value in the grid indicates the final engineering strain of the sample.

		Strain Rate (s^{-1})	
		0.1	**10**
Temperature (°C)	**20**	0.35	0.2
	200	0.5	0.2
	400	0.5	0.2
	600	0.5	0.5
	800	0.5	0.5

The measured load (F) and displacement (ΔL) are converted into the true stress (σ_t) and true strain (ε_t) using equations 1 and 2, respectively. The initial area (A_0) and length (L_0) account for the thermal expansion of the sample.

$$\varepsilon_t = ln\left(1 + \frac{-\Delta L}{L_0}\right) \quad (1)$$

$$\sigma_t = \frac{F}{A_0} exp(\varepsilon_t) \quad (2)$$

3. Experimental Results and Model Development

3.1. Experimental stress-strain curves

The true stress-strain graphs at 0.1 s^{-1} and 10 s^{-1} are shown in Fig. 2a and 2b, respectively. For each test condition, two data

sets are shown in this figure (Sample 1 and Sample 2) to demonstrate the good repeatability achieved. At the strain rate of 0.1 s^{-1}, higher deformation temperatures resulted in reduced flow stresses throughout the entire temperature range tested. In contrast, at $\dot{\varepsilon} = 10$ s^{-1} the flow stress at 400 °C (the orange line in Fig. 2) is slightly higher than at 200 °C (the black line in Fig. 2), which is within the DSA temperature range reported in the literature [5]. Although, it should be noted that none of these flow stress curves demonstrate the Portevin Le Chatelier serrated flow effect that is associated with DSA [5].

The DRX effect is observed at temperatures from 400 °C at 0.1 s^{-1}, and from 600 °C at 10 s^{-1}. The DRX effect was likely not observed at 400 °C at the higher 10 s^{-1} strain rate because the total strain reached was much lower.

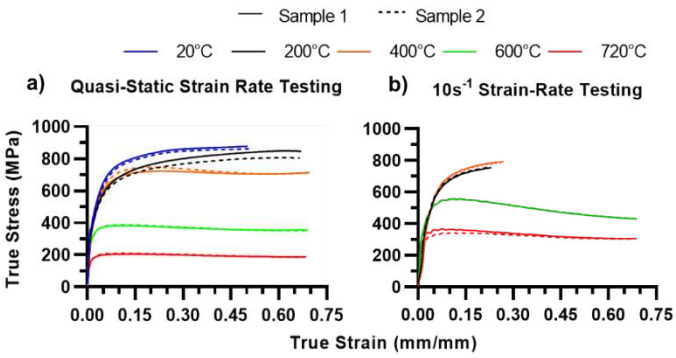

Fig. 2 (a) quasi-static and (b) 10 s^{-1} high temperature compression testing true stress-strain curves. Sample 1 is represented by a solid line and sample 2, the repeat, is represented by a dashed line.

Fig. 3 highlights the non-linear thermal softening effect at 0.1 s^{-1} and 10 s^{-1} testing conditions, represented by the blue and red lines respectively. The material shows a negligible strain rate and thermal softening sensitivity up to 400°C where the flow stresses are almost constant, apart from a slight increase at 400°C in the higher strain rate test. The strain rate sensitivity increases above 400°C and there is a significant reduction in the flow stress as the thermal softening effect becomes dominant.

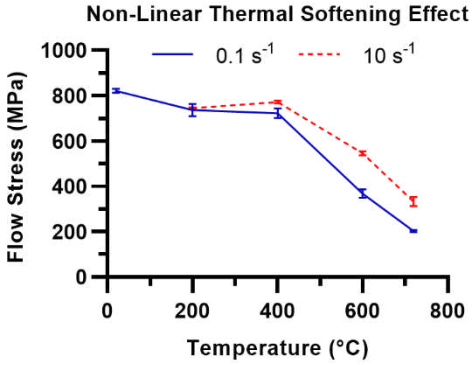

Fig. 3. Non-linear thermal softening effect at strain rates of 0.1 and 10 s^{-1} at a true strain of 0.2. The error bars show the standard deviation.

3.2. Microstructure analysis

SEM micrographs of the central section of the deformed compression samples from 0.1 s^{-1} testing conditions are shown in Fig. 4. The material has a lamellar pearlitic structure up to the testing temperature of 400°C (Fig. 4a, b, and c), which starts to transform to a globular perlite structure at 600°C (highlighted in red in Fig. 4d). The volume fraction of this globular pearlite further increases at 720°C (Fig. 4e). This correlates with the temperature from which the increased rate of thermal softening is observed in Fig. 3. This effect was also observed in the higher 10 s^{-1} strain rate testing.

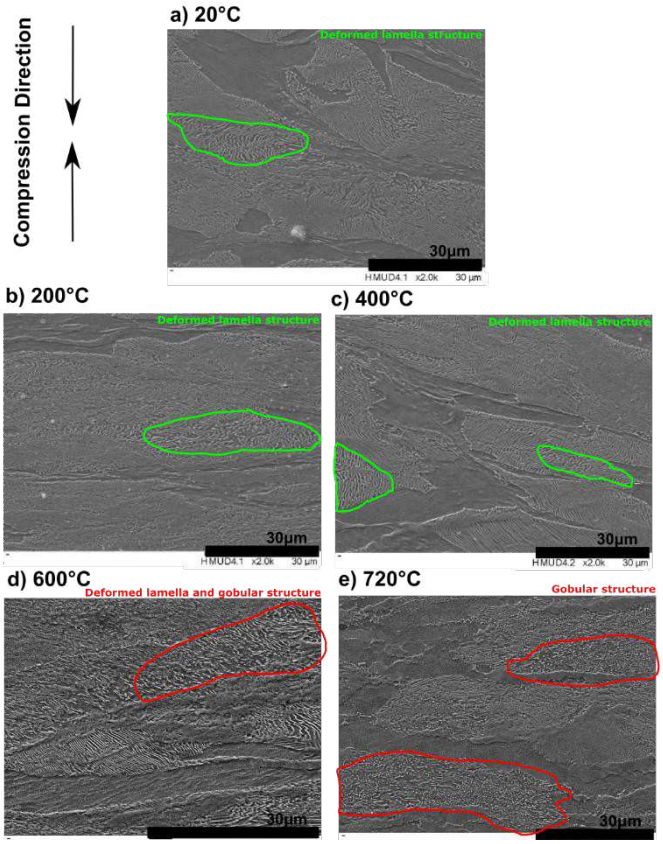

Fig. 4. SEM micrographs at the centre of the 0.1 s^{-1} compression testing at (a) 20°C (b) 200°C, (c) 400°C, (d) 600°C, and (e) 720°C. Green highlights regions of the deformed lamella and red highlights the regions of globular pearlite structure.

3.3. Calibration of the original JC model

The original JC model, shown in Eqn. 3, captures the plastic strain ε_p, plastic strain rate $\dot{\varepsilon}_p$, and temperature T effects on the flow stress. The parameters were determined through a series of linear regression curve fitting steps as outlined by Murugesan and Jung [11]. The tuned JC parameters using the data from the compression testing (detailed in section 3.1) are in Table 3. The original JC model has a poor fit with the experimental flow stress data, shown in Fig. 5, as it does not capture the significant increase in the thermal softening and strain rate sensitivity above 400°C.

$$\sigma_{JC} = \left(A + B{\varepsilon_p}^n\right)\left(1 + C\,ln\left(\frac{\dot{\varepsilon}_p}{\dot{\varepsilon}_0}\right)\right)\left(1 - \left(\frac{T - T_0}{T_m - T_0}\right)^m\right) \quad (3)$$

Table 3. JC model tuned parameters

A (MPa)	B (MPa)	n	C	m	T_0 (°C)	T_m (°C)	$\dot{\varepsilon}_0$ (s^{-1})
334.6	614.94	0.159	0.0075	1.14	20	1350	0.1

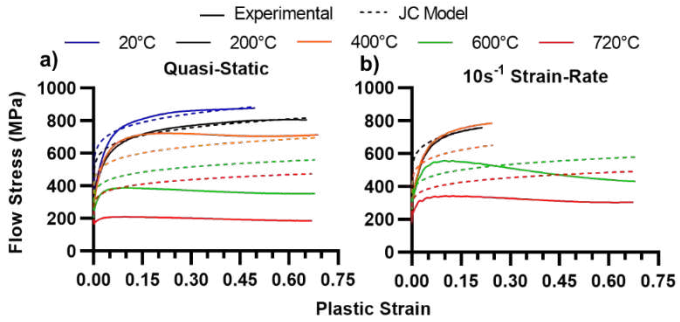

Fig. 5. (a) Experimental flow stress data (solid line) compared with the predicted flow stress using the original JC model (dashed lined) at (a) 0.1 s^{-1} and (b) 10 s^{-1}.

3.4. Modified JC model development

To capture the non-linear thermal softening and strain rate sensitivity effects demonstrated, a modification to the JC model (equation 3) has been implemented. This has been achieved by modifying the strain rate sensitivity (C) and thermal softening (m) parameters to be a function of temperature, as shown in equations 4 and 5. These functions were chosen as they demonstrate a good fit with the experimental data. This modification introduces an additional 4 constants compared to the original JC model, with a_c, b_c, c_c as the strain rate dependent terms and a_m, b_m, c_m as the temperature dependent terms.

$$C(T) = a_c exp\,(b_c T) + c_c \tag{4}$$

$$m(T) = a_m \exp\left(-\left(\frac{T-b_m}{c_m}\right)^2\right) \tag{5}$$

To determine the temperature dependence of the strain rate sensitivity (C) and thermal softening (m) coefficients, these are first calibrated for each test temperature by minimising the error between the experimental and predicted flow stress. Following this, the additional empirical parameters are determined by curve fitting these coefficients with the temperature. This is shown in Fig 6a and Fig 6b for the strain rate sensitivity and thermal softening coefficients, respectively. Fig 6b indicates some strain sensitivity of the thermal softening coefficient which is likely due to the DRX effect that is not captured by the modified JC model.

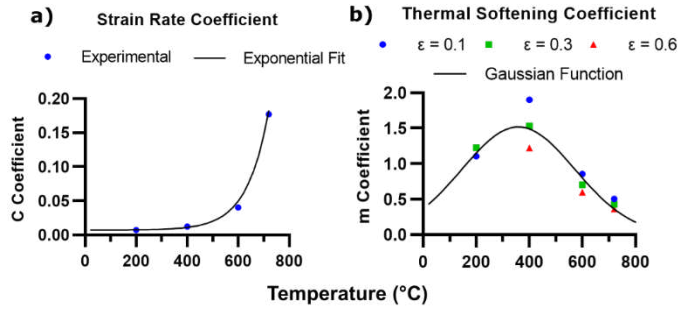

Fig 6. Variation of (a) C and (b) m coefficient with temperature. The fitted model is shown as a solid black line.

Fig 7 demonstrates that the developed model has a better agreement with the measured experimental data compared with the original JC model presented in Fig. 5. A significant improvement is realised at temperatures above 600°C due to the increased strain rate sensitivity and thermal softening effect. The final tuned empirical parameters are presented in Table 4.

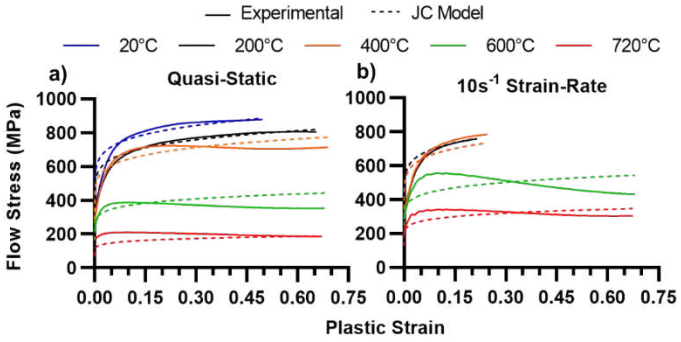

Fig 7. a) Experimental flow stress data (solid line) compared with the predicted flow stress using the modified JC model (dashed lined) at (a) 0.1 s^{-1} and (b) 10 s^{-1}.

Table 4. Modified JC model parameters

A (MPa)	B (MPa)	n	T_0 (°C)	T_m (°C)	$\dot{\varepsilon}_0$ (s^{-1})
334.6	614.94	0.159	20	1350	0.1
a_m	b_m	c_m	a_c	b_c	c_c
1.519	358.9	300.9	3.47 x10^{-5}	0.0118	0.00701

4. Experimental drilling tests and 3D Finite Element Modelling

To further assess the performance of the proposed modified JC model, both the modified and the original JC model were implemented into a 3D drilling simulation and compared with experimental thrust force and torque measurements.

4.1. Experimental drilling test

A 7.5mm diameter CoroDrill 460XM, with through-tool coolant delivery using 7% Hocut 795 emulsion coolant, was used to drill ten 25mm deep blind holes in the same batch of C45U material. The manufactures recommended cutting parameters were used, this is a feed rate of 0.151 mm/rev a surface speed of 109 m/min. This was carried using a DMU 60 Evo 3 axis CNC machine with a Kistler 9171A dynamometer to measure the forces. The averaged experimental thrust and torque measurements in the steady-state engagement region are shown in Table 5.

Table 5. Experimental steady-state drilling thrust force and torque.

	Thrust (N)	Torque (Nm)
Mean	944.5	2.924
Minimum	927.9	2.848
Maximum	967.6	3.002

Fig. 8 shows a cross-section of a produced chip that consists of heavily deformed pearlite and ferrite grains. Fig. 8b demonstrates the formation of globular pearlite (highlighted in red) within the secondary shear zone, which was also observed in the compression testing at temperatures from 600°C.

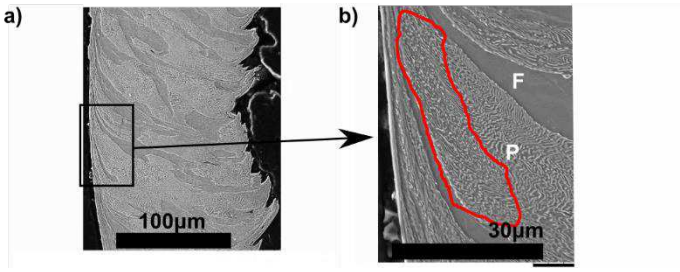

Fig. 8. (a) Cross-section of the prepared chip, and (b) a higher magnification cross-section with globular pearlite highlighted red.

4.2. Modelling Methodology

The updated-Lagrangian with dynamic re-meshing methodology was implemented using the DEFORM 3D implicit finite element software package with a thermally coupled solver. This formulation is reported to be the most reliable, yet computationally affordable 3D modelling methodology, as demonstrated by Priest et al. [12].

A cone-shaped initial workpiece geometry with element sizes ranging from 30 to 60 µm was used to reduce the simulation times. The tool was modelled as a rigid body and a total step time of 0.01 s was simulated to ensure steady-state engagement drilling is reached. The modified JC model was implemented by a FORTRAN user-defined sub-routine (USR_MTR). A damage model was not implemented given that the chip separation was taken care of with continuous re-meshing. The stick-slip friction model with a constant coulomb coefficient of friction of 0.2, and constant limiting shear stress of $A/\sqrt{3}$ was used [12]. Further details of the methodology used and the physical material properties of the workpiece and WC tool used are detailed in [12].

4.3. Modelling Results

Fig.9a and Fig.9b show the predicted transient thrust force and torque response, respectively. The predicted transient thrust forces using the modified and the original JC model are similar up to 0.0085s. After this, once a steady-state is reached, the modified JC predicts a lower thrust force. The predicted transient torque using the modified JC model is much higher with larger fluctuations compared to the original JC model. The fluctuations in the predicted torque correlated to the re-meshing increments, a coarser mesh resulted in a rapid increase of the torque whilst a finer mesh resulted in a rapid decrease of the torque.

The error in the predicted steady-state thrust force and torque compared to the experimentally measured data is shown in Fig.9c. The modified JC model improved the thrust force prediction by approximately 13 % compared with the original JC model; predicting the thrust force to within 19 % compared with the experimental data. The torque predicted using the modified JC model had an error of approximately 40 % compared with the experimental data, whilst the original JC model predicted this to within 9 % of the experimental data.

The addition of a friction model that is dependent on the local thermomechanical contact conditions, which better represents the physics of the problem, will likely further reduce the error in the predicted thrust force and torque compared with the experimental data.

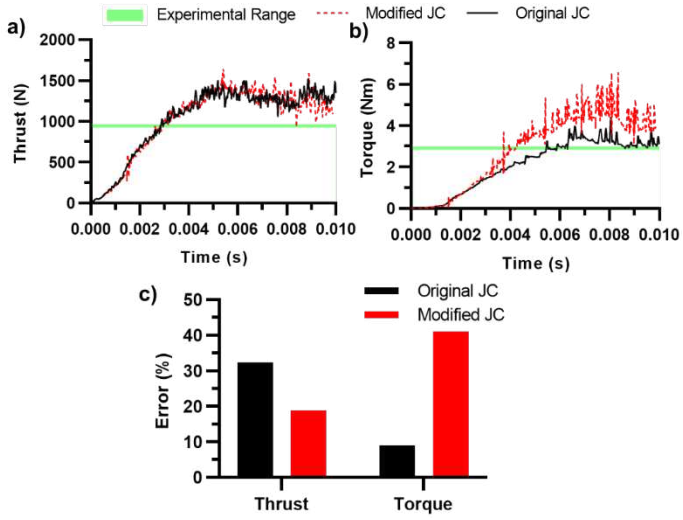

Fig.9. (a) Predicted transient (a) thrust force and (b) torque response, comparing the original JC in the solid black line and the modified JC model in the dashed red line to the experimentally measured range represented by the green band. (c) The average steady-state errors.

The temperatures predicted after 0.008s of engagement are shown in Fig. 10. The modified JC model in Fig. 10b predicts higher temperatures (~565 °C) in the primary and secondary deformation zones by approximately 135°C compared to the original JC model shown in Fig. 10a.

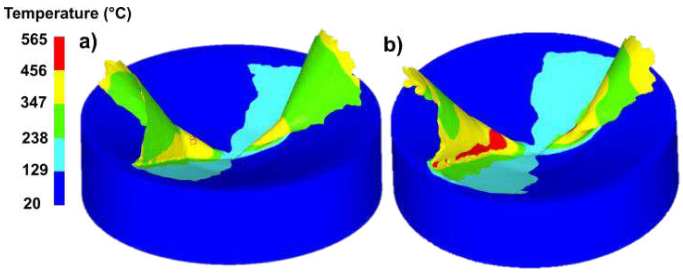

Fig. 10. (a) Original and (b) modified JC model predicted temperature.

5. Discussion

The lower rate of thermal softening below 600°C has been observed by other researchers, which has been attributed to the DSA effect [9][5]. Although, the micrographs of the deformed samples at 600 and 720°C demonstrate that the lamella structure of the carbides in the pearlite grains transforms to a globular structure, which likely also contributes to the significant reduction in flow stress at these temperatures. It should be noted that the Portevin Le Chatelier serrated flow stress effect, which is associated with DSA and observed by Moris et al. [5], was not seen in this study. Additionally, the strain rates used in this study are much lower than the strain rate (3500 s^{-1}) the DSA effect was observed at by Bleicher et al. [9]. However, as the DSA effect is not observable within the microstructure, this cannot be ruled out as a contributing factor.

The predicted temperature in the secondary deformation zone using the modified JC model is around 565 °C, which is very closer to the temperature (600 °C) that globular pearlite

was first observed in the experimental compression tests. As globular pearlite was also observed in the chip, this suggests that the temperatures predicted by the modified JC model are much closer to the actual experimental temperatures. The predicted temperatures using the original model in the secondary deformation zone are around 430 °C, globular pearlite was not observed in the compression testing around this temperature.

The developed model also fits with the experimental flow stress data much better than the original JC model within the strain, strain rate, and temperature ranges tested. Although the maximum strain rate used in this study (10 s^{-1}) is magnitudes below that observed in machining, the JC strain rate sensitivity coefficient below 400°C (0.0075 – 0.012) is very similar to that determined by Jaspers and Dautzenberg [4] using much higher strain rates (7500 s^{-1}).

The modified JC model predicts the drilling thrust force and temperatures more accurately than the original model when used in 3D FE drilling simulations. However, the predicted torque using the modified model has a significant error. This is likely because the implemented re-meshing criteria, which is dependent on the local deformation conditions, caused intermittent fluctuations in the mesh quality throughout the simulation. Further work to improve the re-meshing criteria to prevent this is necessary.

The lack of dynamic recrystallisation prediction is a limitation of the model, as demonstrated in the predicted flow stress curves in Fig 7. This becomes apparent when comparing the predicted flow stress to the experimental data at 600°C and 10 s^{-1} (Fig 7b) where there is a large reduction in the flow stress due to DRX. DRX is neglected in this study as this softening mechanism is not observed during the drilling of C45 using commercially recommended feed rates and surface speeds, as demonstrated in the micrograph of the chip in Fig. 8. Therefore, in its current form, this model is only suitable for drilling simulations. To capture the DRX effect, the strain sensitivity term would require modification.

The developed model is also only valid up to 720 °C, temperatures above this are not expected when drilling at surface speeds from 80 – 150 m/min, and the temperatures predicted by the FE models in this study were also below this.

6. Conclusions

A new modified JC model has been developed to capture the non-linear thermal softening and strain-rate sensitivity effects at temperatures below the austenitisation temperature.

The physical mechanisms responsible for this effect are potentially the dynamic strain ageing effect, although the formation of globular pearlite has also been shown to contribute to the increased rate of thermal softening at temperatures from 600 °C to 720 °C. The formation of globular pearlite was also observed in the chip during drilling.

The developed model fits with the experimental stress-strain data and predicts the drilling thrust force better than the original JC model. Additionally, the predicted temperature in the secondary deformation zone using the modified model is much closer to the temperature at which globular pearlite was first observed in the compression testing. The original JC model predicts much lower temperatures, which is not in line with the observation of globular pearlite in the chip. However, the predicted torque using the modified model had significant error compared with the experimental data. This is likely caused by intermittent poor mesh quality, further work to improve the re-meshing criteria in the 3D FE modelling is necessary to reduce this error.

Currently, this modified JC model is only suitable for drilling simulations at commercially recommended cutting parameters as it does not capture the DRX effect and is limited to a maximum temperature of 720 °C.

Acknowledgements

This research was funded by Sandvik Coromant and EPSRC (EP/L016257/1).

References

[1] S. N. Melkote *et al.*, “Advances in material and friction data for modelling of metal machining,” *CIRP Ann. - Manuf. Technol.*, vol. 66, no. 2, pp. 731–754, 2017.

[2] G. Johnson and W. Cook, “A constitutive model and data for metals subjected to large strains, high strain rates and high temperatures,” in *International Symposium on Ballistics ; 7*, 1983, pp. 541–547.

[3] S. A. Iqbal, P. T. Mativenga, and M. A. Sheikh, “Characterization of machining of AISI 1045 steel over a wide range of cutting speeds. Part 2: Evaluation of flow stress models and interface friction distribution schemes,” *Proc. Inst. Mech. Eng. Part B J. Eng. Manuf.*, vol. 221, no. 5, pp. 917–926, 2007.

[4] S. P. F. C. Jaspers and J. H. Dautzenberg, “Material behaviour in conditions similar to metal cutting: Flow stress in the primary shear zone,” *J. Mater. Process. Technol.*, vol. 122, no. 2–3, pp. 322–330, 2002.

[5] A. Moris *et al.*, “A Modified Johnson-Cook Model for Ferritic-Pearlitic Steel in Dynamic Strain Aging Regime,” *Metals (Basel).*, vol. 9, no. 5, p. 528, 2019.

[6] C. Courbon, T. Mabrouki, J. Rech, D. Mazuyer, F. Perrard, and E. D’Eramo, “Towards a physical FE modelling of a dry cutting operation: Influence of dynamic recrystallization when machining AISI 1045,” *Procedia CIRP*, vol. 8, pp. 516–521, 2013.

[7] S. Nemat-Nasser and W. G. Guo, “Thermomechanical response of HSLA-65 steel plates: Experiments and modeling,” *Mech. Mater.*, vol. 37, no. 2-3 SPEC. ISS., pp. 379–405, 2005.

[8] E. Voce, “The Relationship between Stress and Strain for Homogeneous Deformation,” *J. Inst. Met.*, vol. 74, pp. 537–562, 1948.

[9] F. Bleicher *et al.*, “Considering the influence of heating rate, complex hardening and dynamic strain aging in AISI 1045 machining: experiments and simulations,” *CIRP Ann.*, vol. 70, no. 1, pp. 49–52, 2021.

[10] A. M. Devotta, P. V. Sivaprasad, T. Beno, and M. Eynian, “Predicting continuous chip to segmented chip transition in orthogonal cutting of C45E steel through damage modeling,” *Metals (Basel).*, vol. 10, no. 4, 2020.

[11] M. Murugesan and D. W. Jung, “Johnson cook material and failure model parameters estimation of AISI-1045 medium carbon steel for metal forming applications,” *Materials (Basel).*, vol. 12, no. 4, 2019.

[12] J. Priest, H. Ghadbeigi, S. Avar-Soberanis, and S. Gerardis, “3D finite element modelling of drilling: The effect of modelling method,” *CIRP J. Manuf. Sci. Technol.*, vol. 35, pp. 158–168, 2021.